Journal of Solid Mechanics Vol. 13, No. 4 (2021) pp. 384-398
DOI: 10.22034/jsm.2020.1898690.1585

Dynamic and Vibration Analysis for Geometrical Structures of Planetary Gears

A. Shahabi, A.H. Kazemian *

Department of Mechanical Engineering, University of Sistan and Baluchestan, Zahedan , Iran

Received 30 June 2021; accepted 29 August 2021

ABSTRACT

In industry applications, planetary gear systems are widely used in power transmission systems. In planetary gears, dynamic loads, noise and reduction the structural life are produced by system vibrations. For gear transmission systems, the parametric excitation which introduced by the periodically time–varying mesh stiffness of each gear oscillation is the main source of vibration. Generally, there are two methods to evaluate the gear mesh stiffnesses, the finite element method and the analytical method. In this wok, the periodically time–varying mesh stiffness of planetary gears is investigated. The influence of pressure angles on mesh stiffness of meshing gears is shown and the dynamic model of planetary gear sets is studied. When planets of the single–stage spur planetary gear system are meshed by new planets, the system is converted to special type of system with meshed planets. Vibration for geometrical structures (symmetric and anti–symmetric) of planetary system with meshed planets is investigated. Mesh stiffness of meshing gears by estimation function is obtained and numerical results of natural frequencies and vibration modes are derived.

Keywords : Planetary gear; Vibration; Time–varying mesh stiffness; Dynamic model.

1 INTRODUCTION

GENERALLY, planetary gear systems are classified in two types of single–stage spur planetary gear system and system with meshed planets which planets are meshed with each other. Some advantages of planetary gear systems are: compactness, high torque to weight ratio and low noise. Some other positive points of planetary gears are: small radial bearing loads due to axi–symmetric orientation of planetary gears, high speed reduction in small volumes and also co–axial shaft arrangements. In dynamic model of planetary gears key design parameters are: mesh stiffnesses, bearing (support) stiffnesses, component masses and moments of inertia. The main source of vibrations in planetary gear systems is stiffness coefficients of the periodic time–dependent involvement of the contact between sun–planet and ring–planet. Planetary gears are widely used in the aerospace, aircraft, wind turbine, marine and automotive applications and mining equipment. A nonlinear time–varying dynamic model for gear systems, considering time–varying meshing stiffness and other nonlinearities is investigated in [1,2]. Camacho et al.

*Corresponding author. Tel.: +98 9133426400; Fax.: +98 5431132779.
E-mail address: kazemian@eng.usb.ac.ir (A.H. Kazemian)

[3] presented a methodology to enhance the preliminary design of a single–stage gearbox by diminishing the dynamic load between gears. Chen and Shao [4] introduced a mesh stiffness model of internal gear pair with a tooth root crack in the ring gear based on the potential energy principle. Sun and Ha [5] presented the nonlinear dynamics of a planetary gear system with time–varying mesh stiffnesses and error excitation. A finite element model of the geared rotor system is established by Hao et al. [6] where the rotating beam elements are used and the linear mesh stiffness of engaged helical gears is involved. Inalpolat and Kahraman [7] proposed a nonlinear time–varying dynamic model to predict modulation sidebands of planetary gear sets with periodically time–varying gear mesh stiffnesses and the nonlinearities associated with tooth separations. An advanced model of spur gear transmissions developed by the authors is used to study the influence of carrier planet pin hole position errors on the behavior of the transmission [8]. Jiang and Liu [9] developed analytical models of mesh stiffness for cracked spur gears considering gear body deflection and dynamic simulation. Lin and Parker [10] studied on free vibration of single–stage planetary gear sets and analyzed natural frequencies. Kahraman [11,12] investigated on dynamic and vibration of planetary gear sets and simulation of transient gear contact done by Kazaz et al. [13]. Nonlinear dynamic behavior of spur planetary gears examined using two models [14]: lumped–parameter model and finite element model. Li et al. [15] established a batch module called "integration of finite element analysis and optimum design" by taking gear systems as testing examples. Meanwhile, a dynamic lumped–parameter gear model incorporating the effects of time–varying nonlinearity formulated by Chen et al. [16] to analyze the spur gear rattle response under the idling condition. Lin and Parker [17] studied on free vibration of single–stage planetary gear sets. Liu et al. [18] considered time–varying stiffness and internal and external excitations to analysis of gear system under fractional–order PID control with the feedback of meshing error change rate. Mandol et al. [19] presented a computational approach to predict the load withstanding capacity of a planetary gear assembly. The dynamic scenario of planetary gear analyzed over a reasonable engineering range in terms of rotation speed and torque [20] and Parker [21] studied on effectiveness of planet phasing to suppress planetary gear vibration. Phadatare and Pratiher [22] studied on bifurcation, stability, and route to chaos of nonlinear dynamic of flexible rotor–bearing system. Shu et al. [23] proposed a dynamic optimization approach to improve the dynamic performance of the multi–motor driving transmission system by improving its vibration displacement root mean square value. The dynamic model created using a lumped parameter model of the planetary gearbox by Tatar et al. [24] and the gears and carrier in the planetary gearbox are assumed to be rigid. Wang et al. [25] presented an intelligent fault diagnosis method based on an unsupervised learning algorithm called sparse filtering. Dynamical model of a spur gear pair with time–varying stiffness and static transmission error under uncertainties established in [26,27]. Because the fault features of planetary gear are very weak, Zheng et al. [28] presented a new fault diagnosis method for planetary gear based on image feature extraction. Variation of wear depth on tooth profiles of internal gears determined theoretically in [29]. Finite–element theory [30] associated with the lumped mass method for study on the influence of base excitation on the rotor–rolling bearings supports with rubber damping rings coupling dynamics model presented by Zhu et al. [31].

This work investigates on dynamic and vibration for geometrical structures of planetary gears with symmetric and anti–symmetric rotational structures. For rotational systems, the degrees of freedom of system components in translational directions are negligible and components of the system have freedom only in rotational direction. On the other hand for rotational system, translational bearing stiffnesses lead to infinity for negligible degrees of freedom of components in translational directions. For investigation on planetary gear vibration especially natural frequencies and vibration modes, study on the main source of vibration; i.e., the periodically time–varying mesh stiffness of gears is necessary. So, in this study the periodically time–varying mesh stiffness of gears in the form of Fourier series and finite element method are obtained by polynomial estimation function. The influence of pressure angles on mesh stiffness of meshing gears is investigated. According to results of mesh stifnesses, numerical results of natural frequencies and vibration modes for both symmetric and anti–symmetric systems with meshed planets are derived by mean values of gears mesh stiffness.

2 MODELING OF PLANETARY GEARS DYNAMIC

Two–dimensional (2D) lumped–parameter model of single–stage spur planetary gear system is shown in Fig. 1. Each element such as carrier (*c*), ring (*r*), sun (*s*) and *J* planets is assumed to have rigid behavior, i.e., lumped parameter system. Sun and carrier are connected to the input and output shaft respectively; the external torque and force are applied to the input shaft (τ_s and F_s) and the ring gear is held stationary. Planet bearings are connected to the carrier and they are free to rotate. Mass and moment of inertia of bearings are: m_i and I_i for $i = c, r, s, j$

and $j = p1, p2, ..., J$ where J is number of planets and p denotes to the planet. Bearings are modeled by springs in x and y directions which represent translational bearings stiffness ($K_{ix}, K_{iy}, i = c, r, s$). Rotational bearings stiffness ($K_{i\theta}, i = c, r, s$) are modeled by springs in rotational direction (θ) and stiffnesses for planet bearings are represented by K_j . Translational and rotational coordinates of the carrier, ring and sun are: x_i, y_i and θ_i where $i = c, r, s$. The radial and tangential coordinates are: ξ_j and η_j which are known as translational coordinates of planets center. Rotational coordinate of planets is: $u_j = r_j \theta_j$ and θ_j is planets rotation. In the present model, each element has three degrees of freedom in planar motion: two translations and one rotation, so the system has $3(J+3)$ degrees of freedom. The base radius for bearings of the ring, sun, carrier and planets is shown by $r_i, i = c, r, s, j$. For the carrier bearing, r is radius of the circle which passing through the center of planets. In the present model (Fig. 2), flexibilities of the gear teeth and gear bodies are simulated by springs (reciprocal actions of gear mesh modeled as springs). In Fig. 2, sun–j^{th} planet and ring– j^{th} planet meshes are shown. As an example for mesh of sun–j^{th} planet, the circumferential j^{th} planet location is identified by time varying angle of $\psi_j(t)$ and stiffness between sun and j^{th} planet $(k_{sj}(t))$ acting along the line of action.

In Fig. 2, $k_{rj}(t)$ and $k_{sj}(t)$ are the periodically time–varying mesh stiffness of the ring– j^{th} planet and also sun– j^{th} planet. The basis frequency of the system is ω_T and equal to: $\omega_T = \gamma_s Q_s Q_r / (Q_s + Q_r)$ where γ_s is angular velocity of the sun gear and Q_s and Q_r are numbers of teeth for the sun and ring gears. So the periodically time–varying mesh stiffness of the ring– j^{th} planet and also sun– j^{th} planet in the form of Fourier series are obtained as Eqs. (1) and (2). In Eqs. (1) and (2), h_r and h_s are the number of harmonic acceptable terms to explain and show the periodic functions of $k_{rj}(t)$ and $k_{sj}(t)$. $k_{rp}(t)$ and $k_{sp}(t)$ are the harmonic coefficients of Fourier series with the average amounts of k_{rp}^{1} and k_{sp}^{1} .

$$k_{rj}(t) = k_{rp}^{1} + \sum_{j=1}^{h_r} [(k_{rp}^{2j} \cos(\omega_T t - 2\hat{\Delta}_{rj}\pi) + k_{rp}^{2j+1} \sin(\omega_T t - 2\hat{\Delta}_{rj}\pi)] \quad (1)$$

$$k_{sj}(t) = k_{sp}^{1} + \sum_{j=1}^{h_s} [(k_{sp}^{2j} \cos(\omega_T t - 2\Delta_{sj}\pi) + k_{sp}^{2j+1} \sin(\omega_T t - 2\Delta_{sj}\pi)] \quad (2)$$

In the present model, the phasing (phase angle) of sun– j^{th} planet is Δ_{sj} . The phasing of ring– j^{th} planet is $\hat{\Delta}_{rj}$ which equal to $\Delta_{sj} + \Delta_{sr}$ and Δ_{sr} is the phasing of sun and ring gear (the phase angle between mesh of ring – j^{th} planet and mesh of sun– j^{th} planet). Static transmission error ($e_{sj}(t)$) is involved as dynamic excitation at the mesh spring and pressure angle between sun and j^{th} planet is $\alpha_{sj}(t)$. In Fig. 1, coordinates used in this model are shown and $\psi_j(t)$ depend on the unit vector's rotation (**i** unit vector) and measure counter–clockwise from the first planet, so that $\psi_{p1} = 0$. When planets of the single–stage spur planetary gear system are meshed by new planets, the system is converted to special type of system with meshed planets (planet 1 and planet 2 are meshed with each other, see Figs. 3 and 4). In system with meshed planets for all planets which relating to the carrier, a planet set is considered. In each planet set, planets are modeled as meshed planets which placing in some planet trains. For the carrier bearing of the system with meshed planets, in Fig. 4, r is radius of the circle which passing through the center of planets (r_{c1} for planet 1 and r_{c2} for planet 2). For meshed planets (mesh of planet 1– planet 2), coordination of meshed planets is labeled by angles of β and the circumferential planet 1 location is identified by time–varying angle of $\psi_1(t)$. Each element has three degrees of freedom in planar motion: two translations and one rotation so the systems with meshed planets have degrees of freedom as:

$$3(N_c + N_s + N_r + N_{PT} . N_{PPT}) \quad (3)$$

In Eq. (3), N shows total of elements and PT and PPT denote to planet train and planet per planet train in the planet set.

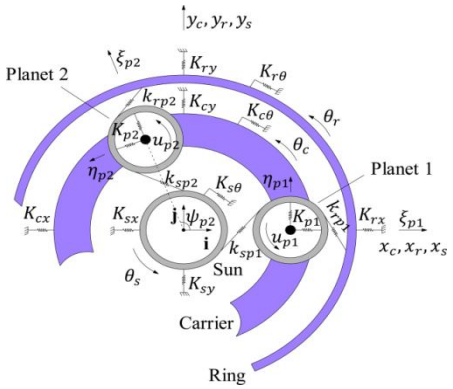

Fig.1
Lumped parameter model of the planetary gear and system coordinates.

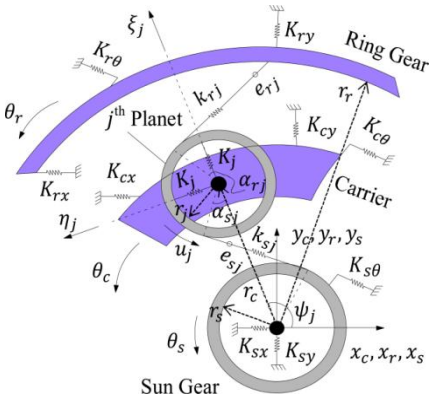

Fig.2
Mesh of the sun, ring and j^{th} planet bearings.

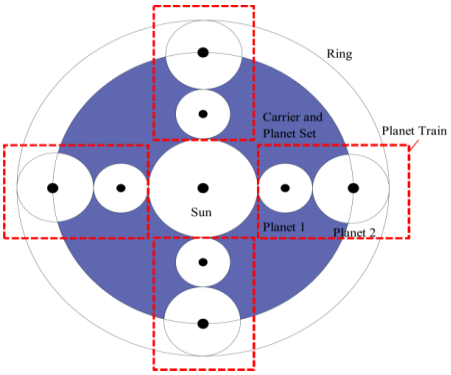

Fig.3
Planetary gear with meshed planets (planet 1 and planet 2 are meshed with each other).

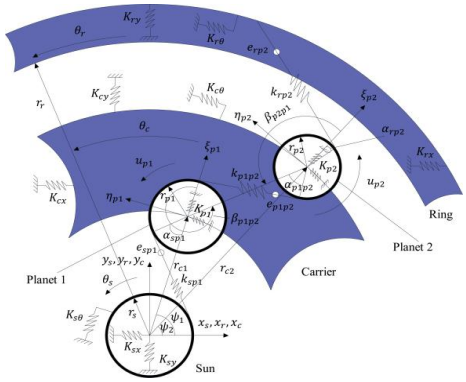

Fig.4
Dynamic model of system with meshed planets (planet 1 and planet 2).

Fig. 5 shows kinematics sketches to derive relative deflection components. As an example, the gear mesh deformation between the sun gear and the j^{th} planet gear (δ_{sj}) is obtained from mixture of the sun and j^{th} planet deflections along the line of action (see Fig. 5(a)). Similarly, the gear mesh deformation between the ring gear and the j^{th} planet gear (δ_{rj}) and the planet bearing radial and tangential interfaces (δ_{jr} and δ_{jt}) with the carrier are derived by kinematics analysis of Figs. 5(b) and 5(c). So compressions of the elastic elements (δ) are defining as Eqs. (4)–(7):

2.1 Sun– j^{th} planet bearings mesh

$$\delta_{sj} = \cos(\psi_j - \alpha_{sj}) y_s - \sin(\psi_j - \alpha_{sj}) x_s - \sin\alpha_{sj}\,\xi_j - \cos\alpha_{sj}\,\eta_j + r_s\theta_s + u_j + e_{sj}(t) \tag{4}$$

2.2 Ring – j^{th} planet bearings mesh

$$\delta_{rj} = \cos(\psi_j + \alpha_{rj}) y_r - \sin(\psi_j + \alpha_{rj}) x_r + \sin\alpha_{rj}\,\xi_j - \cos\alpha_{rj}\,\eta_j + r_r\theta_r - u_j + e_{rj}(t) \tag{5}$$

2.3 j^{th} planet bearing radial

$$\delta_{jr} = \sin\psi_j\, y_c + \cos\psi_j\, x_c - \xi_j \tag{6}$$

2.4 j^{th} planet bearing tangential

$$\delta_{jt} = \cos\psi_j\, y_c - \sin\psi_j\, x_c - \eta_j + r_c\theta_c \tag{7}$$

2.5 Equations of motion

The basic dynamical equilibrium equations contain $3(J+3)$ nonlinear ordinary differential equations. Final equations of motion for single–stage spur planetary gear system of Fig. 1 are obtained by Newton's second law as:

2.5.1 Carrier equations

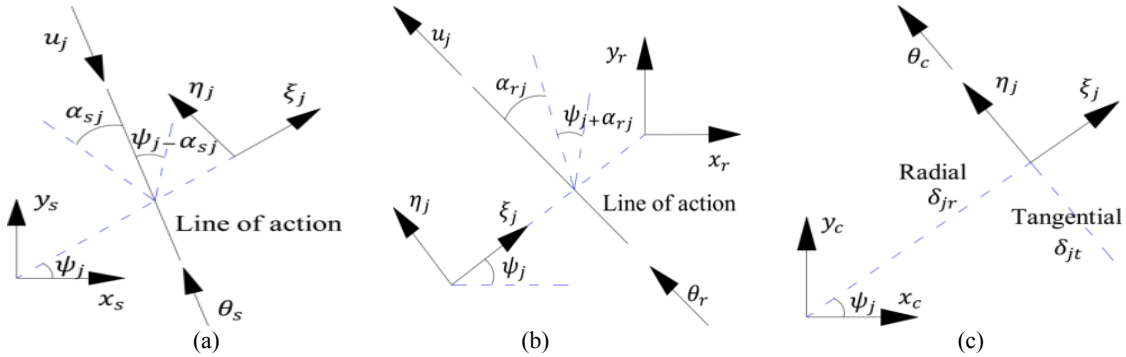

Fig.5
Kinematics sketches to derive relative deflection components.

$$m_c\ddot{x}_c + K_j[(\sin\psi_j(t)\,y_c + \cos\psi_j(t)\,x_c - \xi_j)\cos\psi_j(t) - (\cos\psi_j(t)\,y_c - \sin\psi_j(t)\,x_c - \eta_j + r_c\theta_c)\sin\psi_j(t)] + K_{cy}\,y_c = 0 \tag{8}$$

$$m_c\ddot{y}_c + K_j[(\sin\psi_j(t)y_c + \cos\psi_j(t)x_c - \xi_j)\sin\psi_j(t) + (\cos\psi_j(t)y_c - \sin\psi_j(t)x_c - \eta_j + r_c\theta_c)\cos\psi_j(t)] + K_{cy}y_c = 0 \quad (9)$$

$$I_c\ddot{\theta}_c + K_j(\cos\psi_j(t)y_c - \sin\psi_j(t)x_c - \eta_j + r_c\theta_c) + K_{c\theta}\theta_c = 0 \quad (10)$$

2.5.2 Sun gear equations

$$m_s\ddot{x}_s - k_{sj}(t)(\cos(\psi_j(t) - \alpha_{sj}(t))y_s - \sin(\psi_j(t) - \alpha_{sj}(t))x_s - \sin\alpha_{sj}(t)\xi_j - \cos\alpha_{sj}(t)\eta_j + r_s\theta_s + u_j + e_{sj}(t))\sin(\psi_j(t) - \alpha_{sj}) + K_{sx}x_s = F_{sx}(t) \quad (11)$$

$$m_s\ddot{y}_s + k_{sj}(t)(\cos(\psi_j(t) - \alpha_{sj}(t))y_s - \sin(\psi_j(t) - \alpha_{sj}(t))x_s - \sin\alpha_{sj}(t)\xi_j - \cos\alpha_{sj}(t)\eta_j + r_s\theta_s + u_j + e_{sj}(t))\cos(\psi_j(t) - \alpha_{sj}(t)) + K_{sy}y_s = F_{sy}(t) \quad (12)$$

$$I_s\ddot{\theta}_s + k_{sj}(t)(\cos(\psi_j(t) - \alpha_{sj}(t))y_s - \sin(\psi_j(t) - \alpha_{sj}(t))x_s - \sin\alpha_{sj}(t)\xi_j - \cos\alpha_{sj}(t)\eta_j + r_s\theta_s + u_j + e_{sj}(t)) + K_{s\theta}\theta_s = \tau_s(t) \quad (13)$$

2.5.3 Ring gear equations

$$m_r\ddot{x}_r - k_{rj}(t)(\cos(\psi_j(t) + \alpha_{rj}(t))y_r - \sin(\psi_j(t) + \alpha_{rj}(t))x_r + \sin\alpha_{rj}(t)\xi_j - \cos\alpha_{rj}(t)\eta_j + r_r\theta_r - u_j + e_{rj}(t))\sin(\psi_j(t) + \alpha_{rj}(t)) + K_{rx}x_r = 0 \quad (14)$$

$$m_r\ddot{y}_r + k_{rj}(t)(\cos(\psi_j(t) + \alpha_{rj}(t))y_r - \sin(\psi_j(t) + \alpha_{rj}(t))x_r + \sin\alpha_{rj}(t)\xi_j - \cos\alpha_{rj}(t)\eta_j + r_r\theta_r - u_j + e_{rj}(t))\cos(\psi_j(t) + \alpha_{rj}(t))] + K_{ry}y_r = 0 \quad (15)$$

$$I_r\ddot{\theta}_r + k_{rj}(t)(\cos(\psi_j(t) + \alpha_{rj}(t))y_r - \sin(\psi_j(t) + \alpha_{rj}(t))x_r + \sin\alpha_{rj}(t)\xi_j - \cos\alpha_{rj}(t)\eta_j + r_r\theta_r - u_j + e_{rj}(t)) + K_{r\theta}\theta_r = 0 \quad (16)$$

2.5.4 j^{th} planet equations

$$m_j\ddot{\xi}_j - k_{sj}(t)(\cos(\psi_j(t) - \alpha_{sj}(t))y_s - \sin(\psi_j(t) - \alpha_{sj}(t))x_s - \sin\alpha_{sj}(t)\xi_j - \cos\alpha_{sj}(t)\eta_j + r_s\theta_s + u_j + e_{sj}(t))\sin\alpha_{sj}(t) + k_{rj}(t)(\cos(\psi_j(t) + \alpha_{rj}(t))y_r - \sin(\psi_j(t) + \alpha_{rj}(t))x_r + \sin\alpha_{rj}(t)\xi_j - \cos\alpha_{rj}(t)\eta_j + r_r\theta_r - u_j + e_{rj}(t))\sin\alpha_{rj}(t) - K_{pn}(\sin\psi_j(t)y_c + \cos\psi_j(t)x_c - \xi_j) = 0 \quad (17)$$

$$m_j\ddot{\eta}_j - k_{sj}(t)(\cos(\psi_j(t) - \alpha_{sj}(t))y_s - \sin(\psi_j(t) - \alpha_{sj}(t))x_s - \sin\alpha_{sj}(t)\xi_j - \cos\alpha_{sj}(t)\eta_j + r_s\theta_s + u_j + e_{sj}(t))\cos\alpha_{sj}(t) - k_{rj}(t)(\cos(\psi_j(t) + \alpha_{rj}(t))y_r - \sin(\psi_j(t) + \alpha_{rj}(t))x_r + \sin\alpha_{rj}(t)\xi_j - \cos\alpha_{rj}(t)\eta_j + r_r\theta_r - u_j + e_{rj}(t))\cos\alpha_{rj}(t) - K_j(\cos\psi_j(t)y_c - \sin\psi_j(t)x_c - \eta_j + r_c\theta_c) = 0 \quad (18)$$

$$\frac{I_j}{r_j^2}\ddot{u}_j + k_{sj}(\cos(\psi_j(t) - \alpha_{sj}(t))y_s - \sin(\psi_j(t) - \alpha_{sj}(t))x_s - \sin\alpha_{sj}(t)\xi_j - \cos\alpha_{sj}(t)\eta_j + r_s\theta_s + u_j + e_{sj}(t)) - k_{rj}(t)(\cos(\psi_j(t) + \alpha_{rj}(t))y_r - \sin(\psi_j(t) + \alpha_{rj}(t))x_r + \sin\alpha_{rj}(t)\xi_j - \cos\alpha_{rj}(t)\eta_j + r_r\theta_r - u_j + e_{rj}(t)) = 0 \quad (19)$$

Similarly, for the planetary gear system with meshed planets (system of Figs. 3 and 4 for one planet train with planet 1 and planet 2) the following equations of motion are obtained:

2.5.6 Carrier equations

$$m_c\ddot{x}_c + K_{cx}x_c + [K_{p1}(x_c\cos\psi_1(t) + y_c\sin\psi_1(t) - \xi_{p1})\cos\psi_1(t) - (-x_c\sin\psi_1(t) + y_c\cos\psi_1(t) + r_{c1}\theta_c - \eta_{p1})\sin\psi_1(t)] + [K_{p2}(x_c\cos\psi_2(t) + y_c\sin\psi_2(t) - \xi_{p2})\cos\psi_2(t) - (-x_c\sin\psi_2(t) + y_c\cos\psi_2(t) + r_{c2}\theta_c - \eta_{p2})\sin\psi_2(t)] = 0 \quad (20)$$

$$m_c\ddot{y}_c + K_{cy}y_c + [K_{p1}(x_c\cos\psi_1(t) + y_c\sin\psi_1(t) - \xi_{p1})\sin\psi_1(t) + (-x_c\sin\psi_1(t) + y_c\cos\psi_1(t) + r_{c1}\theta_c - \eta_{p1})\cos\psi_1(t)] + [K_{p2}(x_c\cos\psi_2(t) + y_c\sin\psi_2(t) - \xi_{p2})\sin\psi_2(t) + (-x_c\sin\psi_2(t) + y_c\cos\psi_2(t) + r_{c2}\theta_c - \eta_{p2})\cos\psi_2(t)] = 0 \quad (21)$$

$$I_c\ddot{\theta}_c + K_{c\theta}\theta_c + [K_{p1}(-x_c\sin\psi_1(t) + y_c\cos\psi_1(t) + r_{c1}\theta_c - \eta_{p1})r_{c1}] + [K_{p2}(-x_c\sin\psi_2(t) + y_c\cos\psi_2(t) + r_{c2}\theta_c - \eta_{p2})r_{c2}] = 0 \quad (22)$$

2.5.7 Sun gear equations

$$m_s\ddot{x}_s + K_{sx}x_s - k_{sp1}(t).[y_s\cos(\psi_1(t) - \alpha_{sp1}(t)) - x_s\sin(\psi_1(t) - \alpha_{sp1}(t)) + r_s\theta_s - \xi_{p1}\sin\alpha_{sp1}(t) - \eta_{p1}\cos\alpha_{sp1}(t) + u_{p1} + e_{sp1}(t)]\sin(\psi_1(t) - \alpha_{sp1}(t)] = F_{sx}(t) \quad (23)$$

$$m_s\ddot{y}_s + K_{sy}y_s + k_{sp1}(t).[y_s\cos(\psi_1(t) - \alpha_{sp1}(t)) - x_s\sin(\psi_1(t) - \alpha_{sp1}(t)) + r_s\theta_s - \xi_{p1}\sin\alpha_{sp1}(t) - \eta_{p1}\cos\alpha_{sp1}(t) + u_{p1} + e_{sp1}(t)]\cos(\psi_1(t) - \alpha_{sp1}(t)] = F_{sy}(t) \quad (24)$$

$$I_s\ddot{\theta}_s + K_{s\theta}\theta_s + k_{sp1}(t).[y_s\cos(\psi_1(t) - \alpha_{sp1}(t)) - x_s\sin(\psi_1(t) - \alpha_{sp1}(t)) + r_s\theta_s - \xi_{p1}\sin\alpha_{sp1}(t) - \eta_{p1}\cos\alpha_{sp1}(t) + u_{p1} + e_{sp1}(t)]r_s = \tau_s(t) \quad (25)$$

2.5.8 Ring gear equations

$$m_r\ddot{x}_r + K_{rx}x_r - k_{rp2}(t).[y_r\cos(\psi_2(t) + \alpha_{rp2}(t)) - x_r\sin(\psi_2(t) + \alpha_{rp2}(t)) + r_r\theta_r + \xi_{p2}\sin\alpha_{rp2}(t) - \eta_{p2}\cos\alpha_{rp2}(t) - u_{p2} + e_{rp2}(t)]\sin(\psi_2(t) + \alpha_{rp2}(t)] = 0 \quad (26)$$

$$m_r\ddot{y}_r + K_{ry}y_r + k_{rp2}(t).[y_r\cos(\psi_2(t) + \alpha_{rp2}(t)) - x_r\sin(\psi_2(t) + \alpha_{rp2}(t)) + r_r\theta_r + \xi_{p2}\sin\alpha_{rp2}(t) - \eta_{p2}\cos\alpha_{rp2}(t) - u_{p2} + e_{rp2}(t)]\sin(\psi_2(t) + \alpha_{rp2}(t)] = 0 \quad (27)$$

$$I_r\ddot{\theta}_r + K_{r\theta}\theta_r + k_{rp2}(t).[y_r\cos(\psi_2(t) + \alpha_{rp2}(t)) - x_r\sin(\psi_2(t) + \alpha_{rp2}(t)) + r_r\theta_r + \xi_{p2}\sin\alpha_{rp2}(t) - \eta_{p2}\cos\alpha_{rp2}(t) - u_{p2} + e_{rp2}(t)]r_r = 0 \quad (28)$$

2.5.9 Planet 1 equations

$$m_{p1}\ddot{\xi}_{p1} + K_{p1}(x_c\cos\psi_1(t) + y_c\sin\psi_1(t) - \xi_{p1}) - k_{sp1}(t).[y_s\cos(\psi_1(t) - \alpha_{sp1}(t)) - x_s\sin(\psi_1(t) - \alpha_{sp1}(t)) + r_s\theta_s - \xi_{p1}\sin\alpha_{sp1}(t) - \eta_{p1}\cos\alpha_{sp1}(t) + u_{p1} + e_{sp1}(t)]\sin\alpha_{sp1}(t) - k_{p1p2}(t).[-\xi_{p1}\sin(\beta_{p1p2}(t) - \alpha_{p1p2}(t)) - \xi_{p2}\sin(\beta_{p2p1}(t) - \alpha_{p1p2}(t)) + \eta_{p1}\cos(\beta_{p1p2}(t) - \alpha_{p1p2}(t)) + \eta_{p2}\cos(\beta_{p2p1}(t) - \alpha_{p1p2}(t)) + u_{p1} + u_{p2} + e_{p1p2}(t)]\sin(\beta_{p1p2}(t) - \alpha_{p1p2}(t)) = 0 \quad (29)$$

$$m_{p1}\ddot{\eta}_{p1} - K_{p1}(-x_c \sin\psi_1(t) + y_c \cos\psi_1(t) + r_{c1}\theta_c - \eta_{p1}) + k_{sp1}(t).[y_s \cos(\psi_1(t) - \alpha_{sp1}(t)) - x_s \sin(\psi_1(t) - \alpha_{sp1}(t)) + r_s\theta_s - \xi_{p1}\sin\alpha_{sp1}(t) - \eta_{p1}\cos\alpha_{sp1}(t) + u_{p1} + e_{sp1}(t)]\cos\alpha_{sp1}(t) + k_{p1p2}(t).[-\xi_{p1}\sin(\beta_{p1p2}(t) - \alpha_{p1p2}(t)) - \xi_{p2}\sin(\beta_{p2p1}(t) - \alpha_{p1p2}(t)) + \eta_{p1}\cos(\beta_{p1p2}(t) - \alpha_{p1p2}(t)) + \eta_{p2}\cos(\beta_{p2p1}(t) - \alpha_{p1p2}(t)) + u_{p1} + u_{p2} + e_{p1p2}(t)]\cos(\beta_{p1p2}(t) - \alpha_{p1p2}(t)) = 0 \quad (30)$$

$$\frac{I_{p1}}{(r_{p1})^2}\ddot{u}_{p1} + k_{sp1}(t).[y_s \cos(\psi_1(t) - \alpha_{sp1}(t)) - x_s \sin(\psi_1(t) - \alpha_{sp1}(t)) + r_s\theta_s - \xi_{p1}\sin\alpha_{sp1}(t) - \eta_{p1}\cos\alpha_{sp1}(t) + u_{p1} + e_{sp1}(t)] + k_{p1p2}(t).[-\xi_{p1}\sin(\beta_{p1p2}(t) - \alpha_{p1p2}(t)) - \xi_{p2}\sin(\beta_{p2p1}(t) - \alpha_{p1p2}(t)) + \eta_{p1}\cos(\beta_{p1p2}(t) - \alpha_{p1p2}(t)) + \eta_{p2}\cos(\beta_{p2p1}(t) - \alpha_{p1p2}(t)) + u_{p1} + u_{p2} + e_{p1p2}(t)] = 0 \quad (31)$$

2.5.10 Planet 2 equations

$$m_{p2}\ddot{\xi}_{p2} - K_{p2}(x_c \cos\psi_2(t) + y_c \sin\psi_2(t) - \xi_{p2}) - k_{rp2}(t).[y_r \cos(\psi_2(t) + \alpha_{rp2}(t)) - x_r \sin(\psi_2(t) + \alpha_{rp2}(t)) + r_r\theta_r + \xi_{p2}\sin\alpha_{rp2}(t) - \eta_{p2}\cos\alpha_{rp2}(t) - u_{p2} + e_{rp2}(t)]\sin\alpha_{rp2}(t) - k_{p1p2}(t).[-\xi_{p1}\sin(\beta_{p1p2}(t) - \alpha_{p1p2}(t)) - \xi_{p2}\sin(\beta_{p2p1}(t) - \alpha_{p1p2}(t)) + \eta_{p1}\cos(\beta_{p1p2}(t) - \alpha_{p1p2}(t)) + \eta_{p2}\cos(\beta_{p2p1}(t) - \alpha_{p1p2}(t)) + u_{p1} + u_{p2} + e_{p1p2}(t)]\sin(\beta_{p2p1}(t) - \alpha_{p1p2}(t)) = 0 \quad (32)$$

$$m_{p2}\ddot{\eta}_{p2} - K_{p2}(-x_c \sin\psi_2(t) + y_c \cos\psi_2(t) + r_{c2}\theta_c - \eta_{p2}) + k_{rp2}(t).[y_r \cos(\psi_2(t) + \alpha_{rp2}(t)) - x_r \sin(\psi_2(t) + \alpha_{rp2}(t)) + r_r\theta_r + \xi_{p2}\sin\alpha_{rp2}(t) - \eta_{p2}\cos\alpha_{rp2}(t) - u_{p2} + e_{rp2}(t)]\cos\alpha_{rp2}(t) + k_{p1p2}(t).[-\xi_{p1}\sin(\beta_{p1p2}(t) - \alpha_{p1p2}(t)) - \xi_{p2}\sin(\beta_{p2p1}(t) - \alpha_{p1p2}(t)) + \eta_{p1}\cos(\beta_{p1p2}(t) - \alpha_{p1p2}(t)) + \eta_{p2}\cos(\beta_{p2p1}(t) - \alpha_{p1p2}(t)) + u_{p1} + u_{p2} + e_{p1p2}(t)]\cos(\beta_{p2p1}(t) - \alpha_{p1p2}(t)) = 0 \quad (33)$$

$$\frac{I_{p2}}{(r_{p2})^2}\ddot{u}_{p2} + k_{rp2}(t).[y_r \cos(\psi_2(t) + \alpha_{rp2}(t)) - x_r \sin(\psi_2(t) + \alpha_{rp2}(t)) + r_r\theta_r + \xi_{p2}\sin\alpha_{rp2}(t) - \eta_{p2}\cos\alpha_{rp2}(t) - u_{p2} + e_{rp2}(t)] + k_{p1p2}(t).[-\xi_{p1}\sin(\beta_{p1p2}(t) - \alpha_{p1p2}(t)) - \xi_{p2}\sin(\beta_{p2p1}(t) - \alpha_{p1p2}(t)) + \eta_{p1}\cos(\beta_{p1p2}(t) - \alpha_{p1p2}(t)) + \eta_{p2}\cos(\beta_{p2p1}(t) - \alpha_{p1p2}(t)) + u_{p1} + u_{p2} + e_{p1p2}(t)] = 0 \quad (34)$$

3 NATURAL FREQUENCIES AND VIBRATION MODES

Equations of motion for both planetary systems (single–stage spur planetary system and system with meshed planets) in matrix form are written as follows:

$$\mathbf{M}\ddot{\mathbf{q}}(t) + \left[\mathbf{K_m}(t) + \mathbf{K_b}\right]\mathbf{q}(t) = \boldsymbol{\tau}(t) + \mathbf{F}(t) \quad (35)$$

where, $\boldsymbol{M}$ is inertia matrix, $\mathbf{K_b}$ is diagonal support (bearing) stiffness matrix and $\mathbf{K_m}(t)$ is symmetric stiffness matrix from coupling between components. $\boldsymbol{\tau}(t)$ is external torque applied on the sun gear and $\mathbf{F}(t)$ shows the static transmission error excitation. Vectors of general coordinates for single–stage spur planetary system and system with meshed planets are:

$$\mathbf{q} = [x_c, y_c, \theta_c, x_r, y_r, \theta_r, x_s, y_s, \theta_s, \xi_{p1}, \eta_{p1}, u_{p1}, ..., \xi_J, \eta_J, u_J]^{\mathrm{T}} \quad (36)$$

$$\mathbf{q} = [x_c, y_c, \theta_c, x_r, y_r, \theta_r, x_s, y_s, \theta_s, \xi_{p1}, \eta_{p1}, u_{p1}, \xi_{p2}, \eta_{p2}, u_{p2}, ...]^{\mathrm{T}} \quad (37)$$

Note that in Eqs. (20)–(34) when numbers of planets are increased in the systems, new coordinates are exerted in equations. In order to evaluate natural frequencies, the associated eigenvalue problem of Eq. (35) is:

$$[-\omega_i^2\mathbf{M}+(\mathbf{K}_b+\mathbf{K}_m(t))]\boldsymbol{\varphi}_i=\mathbf{0} \tag{38}$$

where, ω_i are natural frequencies and $\boldsymbol{\varphi}_i$ are vector of vibration modes. For planetary gear systems vibration modes are classified into three types of translational, rotational and planet modes [10]. To evaluate vibration of symmetric planetary gear system with meshed planets, all planet trains in the planet set must be: equally spaced, the same (all properties) and three or more than three numbers. So the system leads to symmetric structure [10] and when positions of planet trains are unequally spaced around the carrier, the system leads to anti–symmetric structure. Note that for planetary gear system with meshed planets, vibration modes are depended on number of components.

4 NUMERICAL RESULTS

Mesh stiffness of gears depends on different factors such as tooth parameters (gears pressure angle), geometric parameters (gears diameter) and material properties and varies with the gears rotation in the mesh cycle. Contact stiffnesses of tooth pairs in some contact points (coefficients of Fourier series), are obtained separately for both external (sun–j^{th} planet) and internal (ring– j^{th} planet) gears by finite element method for some pressure angles, see Fig. 6.

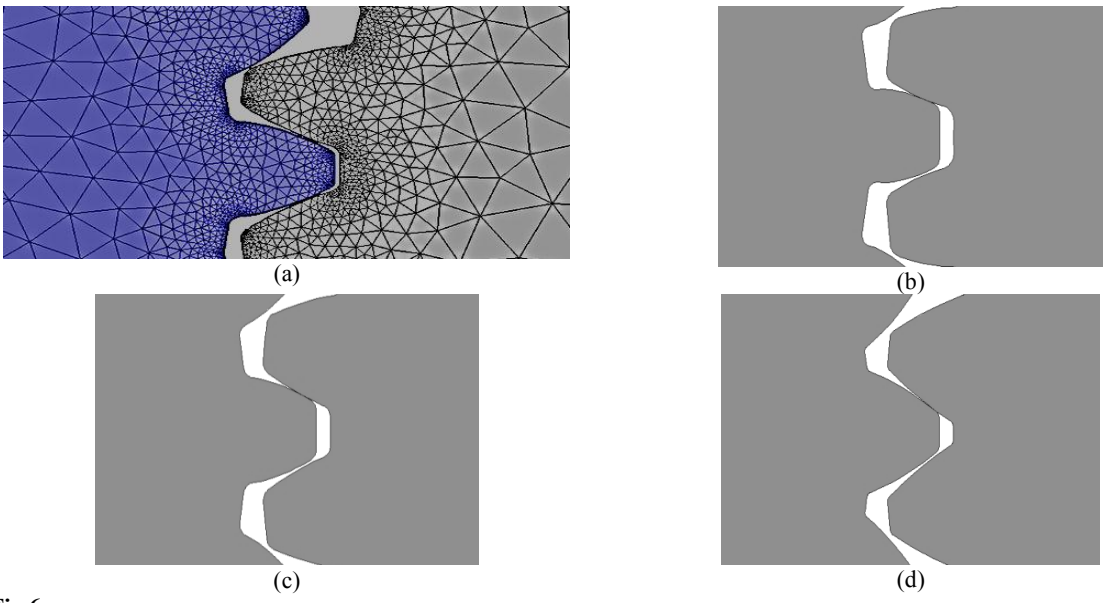

Fig.6
Model of gear meshes by (a) finite element with (b) 20^0 (c) 25^0 and (d) 30^0 pressure angle of gears.

So the periodically time–varying mesh stiffness of the ring– j^{th} planet and also sun– j^{th} planet caused by the change in the number of contact tooth pairs for rotational system in the form of Fourier series is obtained as Eqs. (1) and (2) by polynomial estimation function with system parameters of [10]. Moreover, 206000 $\frac{N}{mm^2}$ for Young's modulus, 0.3 for Poisson's ratio and 7850 kg/m^3 for density and 5 mm for gears modules are considered. All sun– j^{th} planet and ring– j^{th} planet meshes have the same phase ($\Delta_{sj}=\hat{\Delta}_{rj}$). So, all sun– j^{th} planet and ring– j^{th} planet mesh stiffnesses have the same profile. Time–varying mesh stiffness of sun– j^{th} planet and ring– j^{th} planet are shown in Figs. 7 and 8 by estimation function along the line of action. Moreover, in Figs. 7 and 8, the influence of sun– j^{th} planet and ring– j^{th} planet pressure angles on gears mesh stiffness is shown. The influence of the higher pressure angle of gears on mesh stiffness is perceptible. Similarly for the system with meshed planets by parameters of Figs. 9 and 10, time–varying mesh stiffness of sun–planet 1, ring–planet 2 and planet 1–planet 2 are shown in Fig. 11 by estimation function along the line of action. When planets of the single–stage spur planetary gear system are meshed

by new planets, the system is converted to the system with meshed planets which shown in Fig. 3. In Fig. 3, an example of system with meshed planets is presented with four equally spaced planet trains (SS) and in each train; two planets are meshed with each other. Position of each planet in one train has 90 degree deference with planet of other train as Fig. 9. So positions of planet 1 are: 0, 90, 180 and 270 degree and positions of planet 2 are: 40, 130, 220 and 310 degree in four planet trains. Positions of planet 1 and planet 2 in one train can be unequally spaced with planet 1 and planet 2 of other train. It means that the system with meshed planets leads to anti–symmetric structure (ASS). For anti–symmetric system with meshed planets, positions of planet 1 are: 0, 80, 180 and 260 degree and positions of planet 2 are: 40, 120, 220 and 300 degree in four planet trains of this study. According to Eq. (3): $N_c = 1, N_r = 1, N_s = 1, N_{PT} = 4$ and $N_{PPT} = 2$, so the system of Fig. 11 has 33 degrees of freedom and natural frequencies and vibration modes of SS and ASS are tabulated in Table 1.

To evaluate natural frequencies and vibration modes, the system with meshed planets is rotational and system parameters are considered as Figs. 9 and 10. Time–varying mesh stiffness of meshing gears is considered as mean values of Fig. 11 for all planet trains.

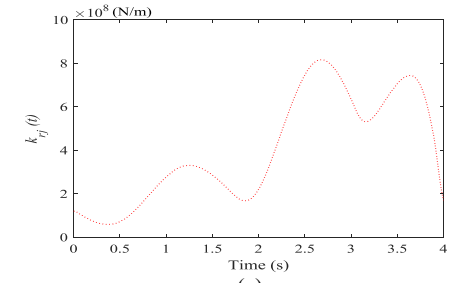

(a)

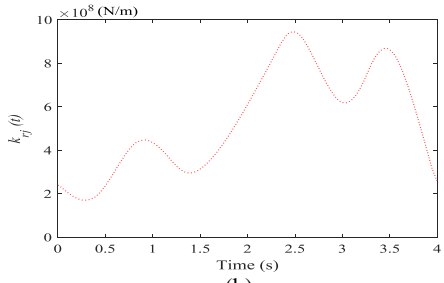

(b)

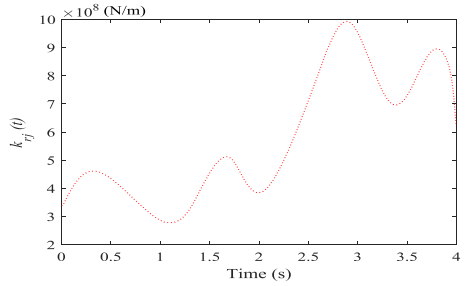

(c)

Fig.7
Mesh stiffness variations of ring–j^{th} planet with (a) $\alpha_{rj} = 20^\circ$, (b) $\alpha_{rj} = 25^\circ$ and (c) $\alpha_{rj} = 30^\circ$.

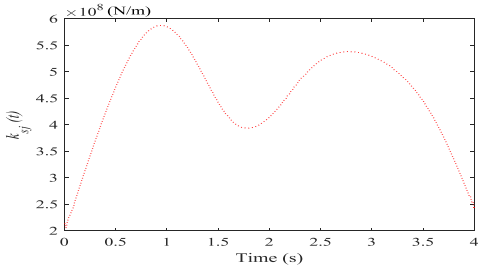

(a)

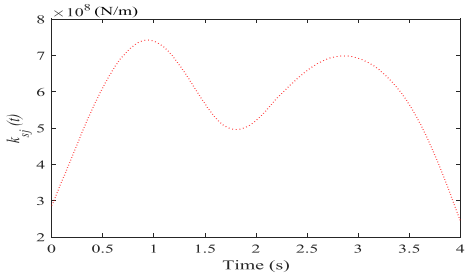

(b)

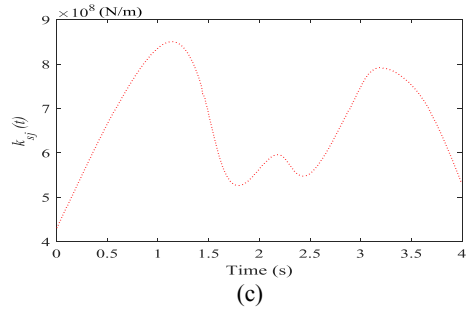

(c)

Fig.8
Mesh stiffness variations of sun–j^{th} planet with (a) $\alpha_{sj} = 20^\circ$, (b) $\alpha_{sj} = 25^\circ$ and (c) $\alpha_{sj} = 30^\circ$.

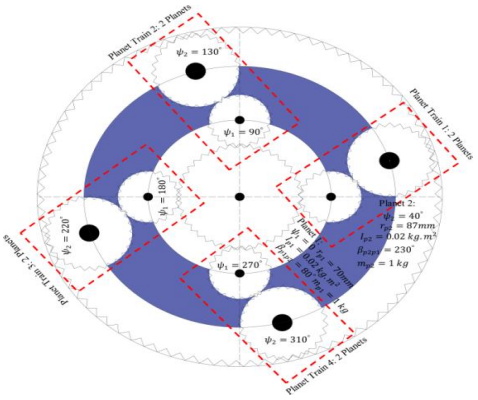

Fig.9
Example of the system with meshed planets and system parameters.

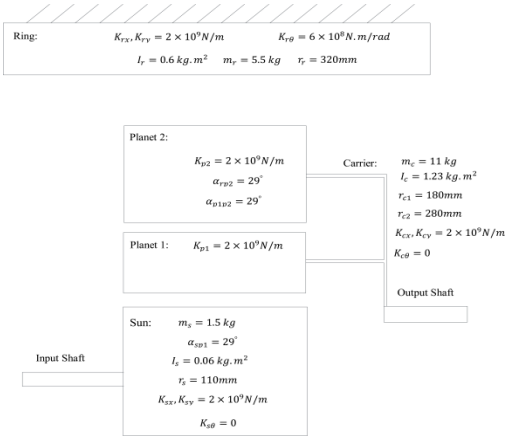

Fig.10
Parameters of the system with meshed planets.

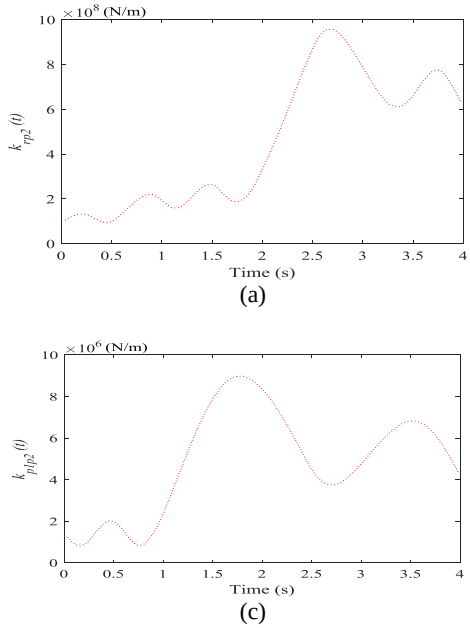

Fig.11
Time–varyin mesh stiffness of (a) sun–planet 1 (b) ring–planet 2 and (c) planet 1 and planet 2 for compound planetary gear system with meshed planets.

Variations of vibration modes for the system with meshed planets and four equally and unequally spaced planet trains are presented in Fig. 12. Moreover, typical vibration mode of the system with meshed planets for SS and ASS are shown in Figs. 13 and 14. Equilibrium and deflected positions are shown by dashed and solid lines. Table 1 for SS shows that, 9 natural frequencies with multiplicity two ($M = 2$ and 18 natural frequencies) have translational modes and 9 and 6 natural frequencies with multiplicity one ($M = 1$) have rotational and planet modes [10]. Unlike the SS, results show for ASS natural frequencies of translational modes have multiplicity one and according to Table

1, 18 natural frequencies with multiplicity one have translational modes and multiplicity of other natural frequencies of ASS is similar to the SS.

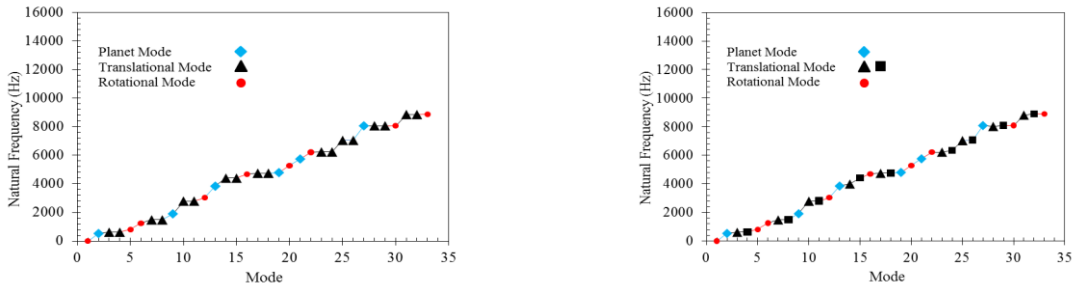

(a) (b)

Fig.12
Variations of vibration modes for the system with meshed planets and four equally (a) and unequally (b) spaced planet trains.

(a) Rotational mode: $\omega_5 = 813.2Hz$

(b) Planet mode: $\omega_2 = 535.1Hz$

(c) Translational mode: $\omega_3 = 613.2Hz$

(d) Translational mode: $\omega_4 = 624.9Hz$

Fig.13
Types of vibration modes of the ASS with four planet trains (planet 1: 0, 80, 180 and 260 degree and planet 2: 40, 120, 220 and 300 degree).

(a) Rotational mode: $\omega_5 = 808.9Hz$

(b) Planet mode: $\omega_2 = 528.7Hz$

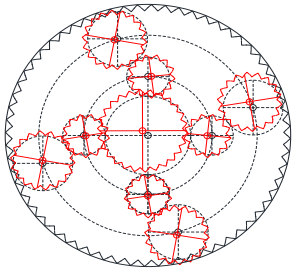

(c) Translational mode:
$\omega_3 = 617Hz$

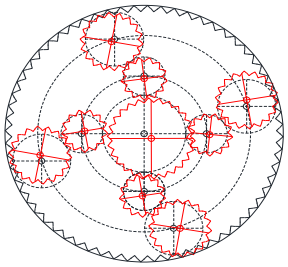

(d) Translational mode:
$\omega_4 = 617Hz$

Fig.14
Types of vibration modes of the SS with four planet trains (planet 1: 0, 90, 180 and 270 degree and planet 2: 40, 130, 220 and 310 degree).

Table 1
Natural frequencies and vibration modes of ASS and SS with four planet trains.

	ASS with four planet trains	SS with four planet trains	Vibration mode
Natural frequencies [HZ] with M=1	0	0	Rotational
	813.2	808.9	Rotational
	1251.8	1245.6	Rotational
	3043.3	3037	Rotational
	4697	4688.4	Rotational
	5289.9	5277.7	Rotational
	6224.1	6213.6	Rotational
	8084.3	8068.4	Rotational
	8891.5	8874	Rotational
Natural frequencies [HZ] with M=2	—	617	Translational
	—	1484.9	Translational
	—	2799.3	Translational
	—	4402.5	Translational
	—	4749.1	Translational
	—	6237	Translational
	—	7049.9	Translational
	—	8067.1	Translational
	—	8857.2	Translational
Natural frequencies [HZ] with M=1	535.1	528.7	Planet
	1912.9	1905.7	Planet
	3851.4	3842.3	Planet
	4804.2	4792.8	Planet
	5758.9	5744.4	Planet
	8082.7	8066.1	Planet
Natural frequencies [HZ] with M=2	613.2, 624.9	—	Translational
	1489, 1478.8		Translational
	2806.1, 2791.9	—	Translational
	4412.6, 3993.5	—	Translational
	4757.1, 4740.3	—	Translational
	6349.3, 6223.8	—	Translational
	7068.3, 7030	—	Translational
	8101.8, 8022.7		Translational
	8901.4, 8814.6		Translational

5 CONCLUSION

In this paper, dynamic and vibration of single–stage spur planetary gear and planetary gear with meshed planets are investigated. For single–stage spur planetary gear the periodically time–varying mesh stiffness of the ring–j^{th} planet and also sun–j^{th} planet in the form of Fourier series and finite element method are obtained by polynomial estimation

function. The influence of gears pressure angle on mesh stiffness of gears is obtained. Similarly, for planetary gear with meshed planets mesh stiffness of meshing gears are obtained by estimation function. For an example of planetary gear with meshed planets, numerical results of natural frequencies and vibration modes are derived by mean values of gears mesh stiffness. According to numerical results, the influence of the higher pressure angle of gears on mesh stiffness is perceptible. Like the structures of the single–stage spur planetary gear system, for structures of the planetary gear system (symmetric and anti–symmetric) with meshed planets, vibration modes are depended on number of system components. It means that characteristics of natural frequencies are similar for both systems.

REFERENCES

[1] Li S., Wu Q., Zhang Z., 2014, Bifurcation and chaos analysis of multistage planetary gear train, *Nonlinear Dynamics* **75**(1-2): 217-233.

[2] Sekar R.P., 2020, A Comparative study of tooth wear, mechanical power losses and efficiency in normal and high contact ratio asymmetric spur gears, *Journal of Solid Mechanics* **12**(1): 148-164.

[3] Camacho-Gutiérrez S., Jáuregui-Correa J.C., Dominguez A., 2019, Optimization of excitation frequencies of a gearbox using algorithms inspired by nature, *Journal of Vibration Engineering & Technologies* **7**: 551-563.

[4] Chen Z., Shao Y., 2013, Dynamic simulation of planetary gear with tooth root crack in ring gear *Engineering Failure Analysis* **31**: 8-18.

[5] Sun T., Hu H., 2003, Nonlinear dynamics of a planetary gear system with multiple clearances, *Mechanism and Machine Theory* **38**(12): 1371-1390.

[6] Hao Z., Xianghe Y., Qingkai H., Hai H., 2019, Dynamic behaviors of geared rotor system in integrally centrifugal compressor, *Journal of Vibration Engineering & Technologies* **7**: 241-249.

[7] Inalpolat M., Kahraman A., 2010, A dynamic model to predict modulation sidebands of a planetary gear set having manufacturing errors, *Journal of Sound and Vibration* **329**: 371-393.

[8] Iglesias M., Fernández A., De-Juan A., Sancibrián R., García P., 2013, Planet position errors in planetary transmission: Effect on load sharing and transmission error, *Frontiers of Mechanical Engineering* **8**(1): 80-87.

[9] Jiang H., Liu F., 2019, Analytical models of mesh stiffness for cracked spur gears considering gear body deflection and dynamic simulation, *Meccanica* **54**: 1889-1909.

[10] Lin J., Parker R.G., 1999, Analytical characterization of the unique properties of planetary gear free vibration, *Journal of vibration and acoustics* **121**: 316-321.

[11] Kahraman A., 1994, Load sharing characteristics of planetary transmissions, *Mechanism and Machine Theory* **29**: 1151-1165.

[12] Kahraman A., 1994, Natural modes of planetary gear trains, *Journal of Sound Vibration* **173**: 125-130.

[13] Kazaz L., Pfister C., Ziegler P., Eberhard P., 2020, Transient gear contact simulations using a floating frame of reference approach and higher-order ansatz functions, *Acta Mechanica* **231**: 1337-1350.

[14] Ambarisha V.K., Parker R.G., 2007, Nonlinear dynamics of planetary gears using analytical and finite element models, *Journal of Sound and Vibration* **302**(3): 577-595.

[15] Li C.H., Chiou H.S., Hung C., Chang Y.Y., Yen C.C., 2002, Integration of finite element analysis and optimum design on gear systems, *Finite Elements in Analysis and Design* **38**(3): 179-192.

[16] Chen Z.G., Shao Y.M., Lim T.C., 2012, Non-linear dynamic simulation of gear response under the idling condition, *International Journal of Automotive Technology* **13**(4): 541-552.

[17] Lin J., Parker R.G., 2001, Natural frequency veering in planetary gears, *Mechanics of Structures and Machines* **29**: 411-429.

[18] Liu L., Niu J., Li X., 2018, Dynamic analysis of gear system under fractional-order PID control with the feedback of meshing error change rate, *Acta Mechanica* **229**: 3833-3851.

[19] Mandol S., Bhattacharjee D., Dan P.K., 2016, Robust optimization in determining failure criteria of a planetary gear assembly considering fatigue condition, *Structural and Multidisciplinary Optimization* **53**: 291-302.

[20] Masoumi A., Pellicano F., Samani F.S., Barbieri M., 2015, Symmetry breaking and chaos-induced imbalance in planetary gears, *Nonlinear Dynamics* **80**: 561-582.

[21] Parker R.G., 2000, A physical explanation for the effectiveness of planet phasing to suppress planetary gear vibration, *Journal of Sound and Vibration* **236**: 561-573.

[22] Phadatare H.P., Pratiher B., 2020, Nonlinear modeling, dynamics, and chaos in a large deflection model of a rotor–disk–bearing system under geometric eccentricity and mass unbalance, *Acta Mechanica* **231**: 1-22.

[23] Shu R., Wei J., Qin D., Lim T.C., Zhang A., 2018, Global sensitivity analysis and dynamic optimization of multi-motor driving transmission system, *Structural and Multidisciplinary Optimization* **58**: 797-816.

[24] Tatar A., Schwingshackl C.W., Friswell M.I., 2019, Dynamic behaviour of three-dimensional planetary geared rotor systems, *Mechanism and Machine Theory* **134**: 39-56.

[25] Wang J., Li S., Xin Y., An Z., 2019, Gear fault intelligent diagnosis based on frequency-domain feature extraction, *Journal of Vibration Engineering & Technologies* **7**: 159-166.

[26] Shen Y., Yang S., Liu X., 2006, Nonlinear dynamics of a spur gear pair with time-varying stiffness and backlash based on incremental harmonic balance method, *International Journal of Mechanical Sciences* **48**(11): 1256-1263.

[27] Wei S., Han Q.K., Dong X.J., Peng Z.K., Chu F.L., 2017, Dynamic response of a single-mesh gear system with periodic mesh stiffness and backlash nonlinearity under uncertainty, *Nonlinear Dynamics* **89**(1): 49-60.

[28] Zheng H., Cheng G., Li Y., Liu C., 2019, A new fault diagnosis method for planetary gear based on image feature extraction and bag-of-words model, *Measurement* **145**:1-13.

[29] Erdin E., Tuc B., Tunalioglu M., 2017, Effect of coating materials on wear in internal Gears, *International Journal of Engineering* **30**(11): 1792-1799.

[30] Lei Y., Hu J., Fu Y., Liu Z., Yan B., 2019, Simulation and experimental study of vibration and noise of pure electric bus transmission based on finite element and boundary element methods, *International Journal of Engineering* **32**(7): 1023-1030.

[31] Zhu H., Chen W., Zhu R., Gao J., Liao M., 2020, Study on the dynamic characteristics of a rotor bearing system with damping rings subjected to base vibration, *Journal of Vibration Engineering & Technologies* **8**: 121-132.